PHYSICAL REVIEW B **82**, 205327 (2010)

Prospect for observing the quantum critical point in double quantum dot systems

Justin Malecki
University of British Columbia, Vancouver, British Columbia, Canada V6T1Z1

Eran Sela
Institute for Theoretical Physics, University of Cologne, 50937 Cologne, Germany

Ian Affleck
University of British Columbia, Vancouver, British Columbia, Canada V6T1Z1

(Received 25 August 2010; published 23 November 2010)

The observation of the quantum critical point in a series double quantum dot system depends on the distinct separation of two scales, $T_K \gg T^*$, where T_K is the Kondo temperature and T^* is the scale at which the system renormalizes away from the quantum critical point to a stable Fermi-liquid fixed point. Using the two-impurity Kondo model, we provide a derivation of T^* based on the renormalization group (RG) to lowest order. This result is confirmed by a numerical RG (NRG) analysis which supplements the analytic derivation with additional quantitative precision. The form of the low-energy Fermi-liquid fixed point is derived and subsequently confirmed by the NRG. From this analysis, we conclude that the aforementioned separation of scales is satisfied, allowing the possibility that the quantum critical point may be measured in a future experiment on such double quantum dot systems.

DOI: 10.1103/PhysRevB.82.205327 PACS number(s): 73.63.Kv, 73.43.Nq

I. INTRODUCTION

Competing orders in correlated electron systems (e.g., heavy-fermion compounds or high-temperature superconductors) lead to new exotic quantum critical points (QCPs). Interestingly, QCPs also occur in much simpler scenarios where correlations are driven fundamentally by a local quantum impurity coupled to a free Fermi sea. One of the most fascinating class of impurity models showing quantum criticality are the multichannel Kondo models.[1] At criticality, the electrons are not described by a Fermi-liquid (FL) theory, as has been demonstrated in quantum dot experiments.[2] However, one element of these critical systems that requires further understanding is the nature of the crossover away from the QCP. This crossover will generically occur due to arbitrarily small symmetry breaking perturbations (such as the presence of a magnetic field in the multichannel Kondo effect) at temperatures small compared to the crossover scale associated with those perturbations.

Therefore, in order to make contact with experiment, an accurate estimate of the crossover energy scale is required. In this paper, we describe such a calculation for a model closely related to multichannel Kondo models, namely, the two-impurity Kondo model which has possible realizations in double quantum dot devices.[3,4] Related experiments on quantum dots[5] or using a scanning tunneling microscope with one impurity on the tip and one on the sample[6] did not observe the physics of the QCP so far. Indeed, theoretical predictions of the influence of the QCP on the nonlinear conductance[7] and shot noise[8] require the crossover energy to be small relative to the Kondo temperature. One of the central purposes of this paper is to clarify and support the possibility of the realization of the QCP in an experiment via a numerical calculation of the crossover scale.

We consider two leads labeled by L and R, each coupled to one of two spin-1/2 "impurities" labeled by $\boldsymbol{S}_L$ and $\boldsymbol{S}_R$, respectively. The two spins are coupled via a Heisenberg exchange interaction K. We also consider a direct tunneling term V_{LR} between the two leads. The system is described by the model Hamiltonian

$$H = \int_{-\infty}^{\infty} dx \sum_{j=L,R} \psi_{j\mu}^{\dagger}(x) i\partial_x \psi_{j\mu}(x) + J(\boldsymbol{s}_{LL}\cdot\boldsymbol{S}_L + \boldsymbol{s}_{RR}\cdot\boldsymbol{S}_R) + K\boldsymbol{S}_L\cdot\boldsymbol{S}_R + V_{LR}[\psi_{L\mu}^{\dagger}(0)\psi_{R\mu}(0) + \psi_{R\mu}^{\dagger}(0)\psi_{L\mu}(0)]. \quad (1)$$

The operator $\psi_{j\mu}(x)$ creates a chiral electron of spin μ at position x in the jth lead (these chiral operators are defined on the entire real line via the standard "unfolding" transformation). We have defined the spin operators $\boldsymbol{s}_{jj} := \psi_{j\mu}^{\dagger}(0)\frac{\boldsymbol{\sigma}_{\mu\nu}}{2}\psi_{j\nu}(0)$ ($\boldsymbol{\sigma}$ are the Pauli matrices) which couple to each impurity spin. The relationship between this Kondo Hamiltonian, which uses spin impurities, to that of a Hamiltonian using Anderson model impurities is detailed in Sec. IV.

Although it is likely that potential scattering terms of the form $V_{LL}\psi_{L\mu}^{\dagger}(0)\psi_{L\mu}(0)$ and $V_{RR}\psi_{R\mu}^{\dagger}(0)\psi_{R\mu}(0)$ will be present in any experimental realization of this model, we neglect such terms as these are marginal at the critical point[4,7] and so will not strongly influence the crossover scale that is the subject of this paper.

For the special case of $V_{LR}=0$, it is known[9] that a quantum critical point separating two distinct Fermi-liquid phases exists for a critical value of $K=K_c \sim T_K$. T_K is the Kondo temperature which we take to be

$$T_K = D\sqrt{\nu J}e^{-1/\nu J}, \quad (2)$$

where $2D$ is the bandwidth or ultraviolet cutoff and $\nu = 1/(2\pi)$ is the density of states in the leads at the Fermi energy (recall that, in our units, the Fermi velocity is $v_F=1$). Throughout this paper, we use $k_B=1$, measuring temperature

in energy units. For $K=K_c$, the effective low-energy model cannot be described as a Fermi liquid. We use the following nomenclature to describe the three phases of the model at $V_{LR}=0$:

$$K < K_c \quad \text{Kondo screened phase (KSP)},$$

$$K = K_c \quad \text{quantum critical point (QCP)},$$

$$K > K_c \quad \text{local singlet phase (LSP)}.$$

For K close to K_c and V_{LR} close to 0 (the meaning of "close" will be defined shortly), the effective description of the system will depend on the temperature T. For $T \gg T_K$, the spins are only weakly coupled to the leads. For $T^* \ll T \ll T_K$, the system will be described by the QCP while, for $T \ll T^*$, the system will be described by a Fermi liquid that is continuously related to the KSP or the LSP via the parameter V_{LR} as will be described in detail in Sec. III.

It has been proposed[7] that the temperature scale T^* can be estimated as

$$T^* = a\frac{(K-K_c)^2}{T_K} + bT_K(\nu V_{LR})^2, \tag{3}$$

where we have inserted two dimensionless numbers a and b that are expected to be of order unity. The value of T^* determines how close K must be to K_c and how close V_{LR} must be to 0 in order to observe the QCP: the values must be such that $T^* \ll T_K$.

To understand where this estimate for T^* comes from, let us assume that K is tuned close to K_c and that νV_{LR} is very small. We want to estimate the crossover energy scale at which the system renormalizes away from the critical point, due to both $\delta K \equiv K-K_c$ and also νV_{LR}. To make a rough estimate, we use the lowest order weak-coupling renormalization group (RG) at energy scales above T_K and the RG at the QCP below T_K. At weak coupling, δK has dimension 1 and νV_{LR} is dimensionless. Thus, at scale T_K,

$$\delta K(T_K) \approx (D/T_K)\delta K,$$

$$\nu V_{LR}(T_K) \approx \nu V_{LR}. \tag{4}$$

Here, the quantities on the right are the bare ones at scale D and the quantities on the left are the renormalized ones at scale T_K. At energy scales $E<T_K$, both δK and νV_{LR} have dimension 1/2 so

$$\delta K(E) \approx (D/T_K)(T_K/E)^{1/2}\delta K,$$

$$\nu V_{LR}(E) \approx (T_K/E)^{1/2}\nu V_{LR}. \tag{5}$$

We estimate the crossover energy scale $T_{\delta K}$ associated with the coupling δK (not to be confused with the Kondo temperature T_K) by setting $\delta K(T_{\delta K})/D \approx 1$. Similarly, we estimate the crossover energy scale T_{LR} associated with the potential scattering by setting $\nu V_{LR}(T_{LR}) \approx 1$. Thus

$$T_{\delta K} \approx a(\delta K)^2/T_K,$$

$$T_{LR} \approx b(\nu V_{LR})^2 T_K, \tag{6}$$

where the dimensionless factors a and b are used to account for quantitative details missed by this simplified analysis. The total crossover scale is then given by $T^*=T_{\delta K}+T_{LR}$. We might expect further modifications if we took into account higher order terms in the RG equations at weak coupling and in the vicinity of the QCP. Hopefully this just leads to corrections which are logarithmic in the dimensionless parameters.

The estimate of Eq. (3) agrees with similar analytic arguments[3,4] (although it is slightly smaller than that found in the latter reference). However, this form of T^* is much smaller than that found using numerical RG (NRG) techniques.[10,11] Given this disagreement, we present in Sec. II a transparent and systematic NRG study with the aim of estimating this crossover scale. We find satisfactory agreement with Eq. (3), contrary to that found in Refs. 10 and 11, though with the magnitude of the coefficients a and b differing from unity. We also find evidence that the coefficient b may have some residual dependence on the Kondo coupling J that is not explained by the simple scaling analysis that lead to Eq. (3).

In Sec. III, we derive the Fermi-liquid theory for the stable low-energy fixed point which is parametrized by the value of V_{LR}. The resulting theory is described in terms of a boundary condition at the origin which can be related to a scattering phase shift. The formula for this phase shift is predicted analytically and supported by comparison with the phase shift derived from the NRG.

II. ESTIMATING T^* USING THE NRG

The numerical renormalization group is a powerful, nonperturbative algorithm for studying quantum impurity systems. It was originally developed to study single-impurity models[12–14] where the technique is exhaustively described. It has since been applied to numerous other impurity problems[15] including the two-impurity problem that we study here.[9] We refer the reader to these references for details on the implementation of the NRG and only review those elements necessary for calculating T^*.

The key idea of the NRG is to approximate the original Hamiltonian describing the leads by that of two semi-infinite tight-binding "Wilson chains,"

$$\begin{aligned}\frac{H}{D} = {} & \frac{1}{2}(1+\Lambda^{-1})\sum_{n=0}^{\infty}\sum_{p=e,o}\Lambda^{-n/2}\xi_n(f_{np\mu}^{\dagger}f_{n+1,p\mu}+\text{H.c.}) \\ & + \nu J\sum_{p=e,o} f_{0p\mu}^{\dagger}\frac{\boldsymbol{\sigma}_{\mu\nu}}{2}f_{0p\nu}\cdot(\boldsymbol{S}_L+\boldsymbol{S}_R) \\ & + \nu J\left(f_{0e\mu}^{\dagger}\frac{\boldsymbol{\sigma}_{\mu\nu}}{2}f_{0o\nu}+\text{H.c.}\right)\cdot(\boldsymbol{S}_L-\boldsymbol{S}_R) \\ & + \frac{K}{D}\boldsymbol{S}_L\cdot\boldsymbol{S}_R + 2\nu V_{LR}(f_{0e\mu}^{\dagger}f_{0e\mu}-f_{0o\mu}^{\dagger}f_{0o\mu}).\end{aligned} \tag{7}$$

Each of the $f_{np\mu}$ operators are complicated linear combinations of $\psi_{e\mu}\sim\psi_{L\mu}+\psi_{R\mu}$ for $p=e$ and $\psi_{o\mu}\sim\psi_{L\mu}-\psi_{R\mu}$ for p

$=o$ (see Ref. 9 for more details). Here, $2D$ is the bandwidth cutoff, $\Lambda>1$ is a numerical parameter (we use $\Lambda=3$), and $\xi_n\sim 1$ is a dimensionless function of Λ. The limit $\Lambda\to 1$ recovers the original model, albeit in a discrete basis.

To simulate the RG flow numerically, one introduces a series of dimensionless Hamiltonians by truncating the semi-infinite chains to $N+1$ sites each and setting the overall energy scale to be of order unity,

$$H_N = \Lambda^{(N-1)/2}\Bigg\{\sum_{n=0}^{N-1}\sum_{p=e,o}\Lambda^{-n/2}\xi_n(f^\dagger_{np\mu}f_{n+1,p\mu}+\text{H.c.}) + \tilde{J}\sum_{p=e,o} f^\dagger_{0p\mu}\frac{\boldsymbol{\sigma}_{\mu\nu}}{2}f_{0p\nu}\cdot(\boldsymbol{S}_L+\boldsymbol{S}_R) + \tilde{J}\left(f^\dagger_{0e\mu}\frac{\boldsymbol{\sigma}_{\mu\nu}}{2}f_{0o\nu}+\text{H.c.}\right)\cdot(\boldsymbol{S}_L-\boldsymbol{S}_R)+\tilde{K}\boldsymbol{S}_L\cdot\boldsymbol{S}_R + \tilde{V}_{LR}(f^\dagger_{0e\mu}f_{0e\mu}-f^\dagger_{0o\mu}f_{0o\mu})\Bigg\}. \tag{8}$$

The parameters $\tilde{J}$, $\tilde{K}$, and $\tilde{V}_{LR}$ are rescaled versions of J, K, and V_{LR} such that

$$\frac{H}{D}=\lim_{N\to\infty}\frac{1}{2}(1+\Lambda^{-1})\Lambda^{-(N-1)/2}H_N. \tag{9}$$

The RG transformation is realized by numerically diagonalizing the series of Hamiltonians H_N, starting with $N=0$, using the lowest[16] eigenvalues (and associated eigenvectors) of H_N to define the H_{N+1} matrix, until the energy spectrum ceases to change from one iteration to the next.[17] The energy scale of the spectrum of the dimensionless H_N is of order unity, meaning that it describes H at a temperature scale T_N given by Eq. (9) to be

$$T_N\sim\frac{1}{2}(1+\Lambda^{-1})\Lambda^{-(N-1)/2}D. \tag{10}$$

This identification will allow us to use the flow of the NRG energy levels to measure the energy scale T^*. Herein, we will take $D=1$ and measure all energy quantities in units of D.

To see how this works in practice, consider the flow of energy levels when the Hamiltonian parameters have been tuned close to the quantum critical point. A few such energy levels have been plotted in Fig. 1. The energy levels flow close to those of the unstable QCP but eventually flow to a stable fixed point (for $V_{LR}=0$ it is either the LSP or KSP depending on the initial value of K; see black solid lines) at an iteration number N^*. We identify the KSP and the LSP by looking at the quantum numbers and degeneracy of the energy levels in each fixed point regime and comparing to those expected from the Wilson chain forms of the fixed-point Hamiltonians.[9] This is not possible for the QCP which does not allow a simple Hamiltonian form. Identifying the spectrum of the QCP requires more sophisticated techniques.[18]

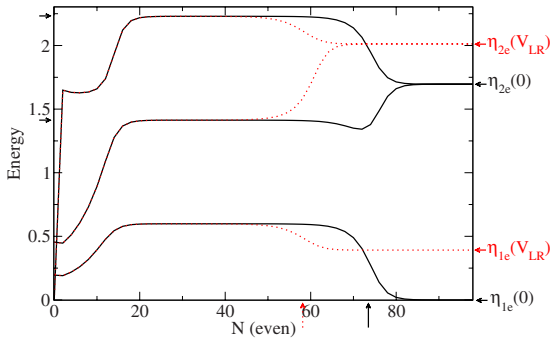

FIG. 1. (Color online) The lowest three NRG energy levels in the charge +1, spin-1/2, parity-even subspace as a function of even iteration parameter N. A value of $\nu V_{LR}=0$ was used to determine the solid lines whereas a value of $\nu V_{LR}=3.372\times10^{-7}$ was used for the dotted lines. The arrows on the left axis label the prediction of the second and third excitation of the QCP from Ref. 18 (the first excitation is used to match the overall scale of the predicted spectrum with that from the NRG). The arrows on the right axis label the first and second single-particle excitations used in the determination of the even channel phase shift, Eq. (21). The arrows on the bottom axis label the value of $\langle N^*\rangle$ used to estimate T^* for each of the two spectra. Here, $\nu J=0.15$ and $K=1.30096478\times10^{-3}>K_c$ so that the final, stable fixed point is that of the LSP.

Quantitatively, we measure the value of N_i^* when the ith energy level crosses over from its QCP value to its stable fixed-point value, then take the average $\langle N_i^*\rangle$ of the values N_i^* for the first 20 energy levels. The resultant value of T^* is determined from Eq. (10) to be

$$T^*=\frac{1}{2}(1+\Lambda^{-1})\Lambda^{-(\langle N_i^*\rangle-1)/2}. \tag{11}$$

To estimate the value of a in Eq. (3), we set $V_{LR}=0$ so that $T^*=T_{\delta K}$ and choose a value of νJ. We then obtain NRG spectra for a series of Hamiltonians with differing values of K, starting with[19] $K=K_c$ then tuning K away from K_c until $T^*\sim T_K$ (i.e., when the QCP is no longer reached in the RG). From these spectra, T^* is extracted as described above and a plot is made of $\ln T^*$ vs $\ln[(K-K_c)^2/T_K]$; see Fig. 2. A linear

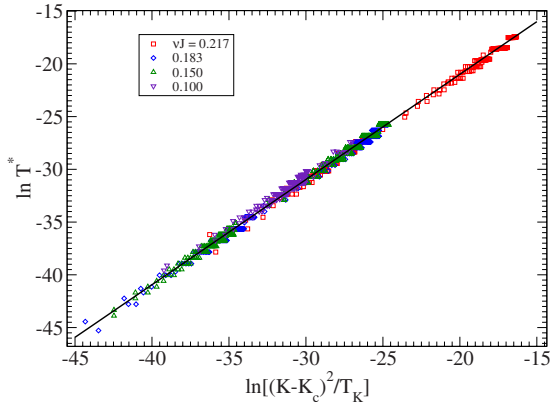

FIG. 2. (Color online) Data for T^* as determined from the NRG with $V_{LR}=0$. The solid line is the best linear fit to all of the data.

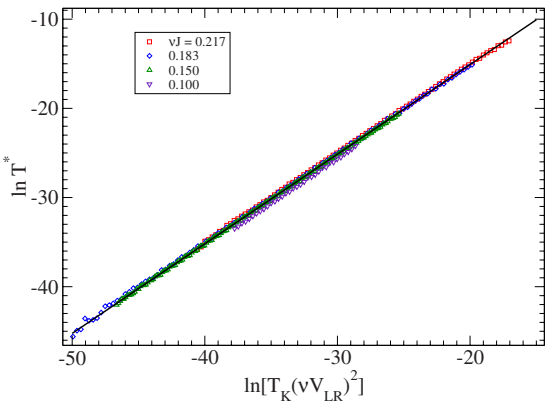

FIG. 3. (Color online) Data for T^* as determined from the NRG with $K=K_c$. The solid line is the best linear fit to all of the data.

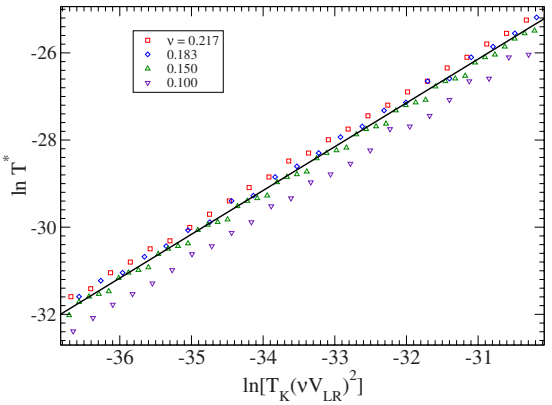

FIG. 4. (Color online) An enlarged version of a section of Fig. 3.

fit is made to the data and compared with the expectation from Eq. (3),

$$\ln T^* = m_a \ln \frac{(K-K_c)^2}{T_K} + \ln a, \quad V_{LR}=0, \tag{12}$$

where T_K is determined from the input value of νJ using Eq. (2). Obtaining the slope $m_a=1$ from the fit provides a check on the dependence of T^* on $K-K_c$ while the intercept of the fit provides an estimate of the dimensionless coefficient a.

A similar procedure is used to measure b. With $K=K_c$ so that $T^*=T_{LR}$, NRG data is obtained for a series of values of V_{LR}, starting with $V_{LR}=0$ and increasing V_{LR} until $T^* \sim T_K$. A plot is made of $\ln T^*$ vs $\ln[T_K(\nu V_{LR})^2]$; see Fig. 3. Again, a linear fit is made to the data and compared with the expectation from Eq. (3),

$$\ln T^* = m_b \ln[T_K(\nu V_{LR})^2] + \ln b, \quad K=K_c. \tag{13}$$

As before, obtaining the slope $m_b=1$ provides a check on the dependence of T^* on νV_{LR} and the intercept determines the value of b. Consistent values of a and b over several values of νJ provide confirmation of the proposed crossover energy scale, Eq. (3).

We have carried out the procedure described above for four values of νJ. The parameters a and b are tabulated in Table I together with the error arising from the fit to the data. In Figs. 2 and 3 we have plotted the data for all four of these iterations and find reasonably good data collapse.

Before describing our analysis of T^*, it is interesting to note that, although we find that $K_c \sim T_K$ as is often quoted in the literature, we do not find the consistent value of $K_c = 2.2T_K$ as reported in Ref. 9. Rather, we find $K_c=\alpha(\nu J)T_K$, where α ranges monotonically (at least according to the four values obtained and listed in Table I) from $\alpha(0.217)=3.36$ to $\alpha(0.100)=1.8$. Although this does not change our conclusions regarding T^*, we simply point out that the relation between K_c and T_K may not be as simple as first presented.[9]

Returning to our analysis of T^*, it is seen that, while the value of a is roughly of order unity, the value of b here is two orders of magnitude larger than unity. Furthermore, while the values of a appear to be consistent for all values of νJ, there seems to be a slight trend of b decreasing with decreasing J. This can be seen in Fig. 4 which is simply an enlarged area of Fig. 3. The fact that we consistently obtain $m_b \approx 1$ means that the T^* dependence on νV_{LR} is certainly quadratic but that the J dependence of the coefficient in the second term of Eq. (3) may be different than that included in the factor of T_K.

For further analysis, we look at the explicit J dependence of the coefficient of $(\nu V_{LR})^2$ in Eq. (3) to see how well it matches that of the predicted bT_K. To do this, we set $K=K_c$ and plot in Fig. 5 the value of $T^*/(\nu V_{LR})^2$ extrapolated to $\nu V_{LR}=0$ for each of the four data sets versus the corresponding value of νJ.[20] To this data we have fit a function of the form

$$\frac{T^*}{(\nu V_{LR})^2} = bT_K = b\sqrt{\nu J}e^{-1/\nu J} \tag{14}$$

and obtained a value of $b=118$. This value is close to the mean of the four values of b listed in Table I and the above function provides a reasonable fit to the data. However, as

TABLE I. NRG results for four values of νJ. Note that all temperatures are measured in units of D with $2D$ being the bandwidth in the leads. The dimensionless parameters a and b are defined in Eq. (3) and Δx indicates the error in x arising from the linear regression.

νJ	T_K ($\times 10^{-3}$)	K_c ($\times 10^{-3}$)	m_a	Δm_a	a	Δa	m_b	Δm_b	b	Δb
0.217	4.644	15.6194231	1.004	0.004	0.35	0.04	0.994	0.001	130	6
0.183	1.811	5.55847415	0.999	0.005	0.33	0.05	0.997	0.002	125	8
0.150	0.4929	1.30096469	1.001	0.004	0.37	0.04	0.999	0.001	114	3
0.100	0.01436	0.02617379	0.99	0.01	0.4	0.2	1.009	0.004	100	14

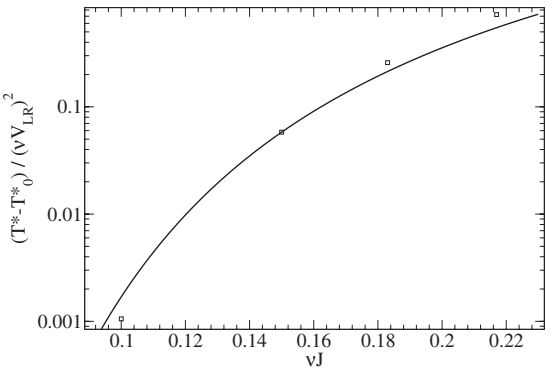

FIG. 5. The value of $T^*/(\nu V_{LR})^2$ extrapolated to $\nu V_{LR}=0$ for each of the four data sets (points). Here, $K=K_c$. A function of the form of Eq. (14) is fit to the data (solid line) with the free parameter found to be $b=118$.

before, there is a hint of further J dependence as the function appears to overestimate the $\nu J=0.1$ data while underestimating the data at $\nu J=0.217$.

III. FERMI-LIQUID THEORY

Having determined the two energy scales T_K and T^*, the latter with aid from the NRG, one can perform perturbative calculations in wide temperature ranges using effective theories appropriate for each regime. In the high-temperature weak-coupling regime $T \gg T_K$, one can apply perturbation theory in J to the original model described by the Hamiltonian of Eq. (1). In the intermediate temperature QCP, $T^* \ll T \ll T_K$, one should use the conformal field theory[21] (or the corresponding theory in the language of Abelian bosonization[22]) and apply perturbation theory in the irrelevant operator. In the low-temperature FL phase, $T \ll T^*$, one can use a Fermi-liquid theory in terms of single fermion scattering states as briefly reported in Ref. 8.

In this section we shall give a derivation of the effective FL Hamiltonian [see Eq. (31)]. In Sec. III A, we derive the phase shift which characterizes the Fermi-liquid fixed point, and which depends on the ratio $(K-K_c)/[T_K \nu V_{LR}]$. This is done using only the formula for the $T=0$ conductance on the line of Fermi-liquid fixed points derived in Ref. 7, a standard Fermi-liquid formula for the conductance in terms of the phase shift, and a symmetry argument. In Sec. III B, we derive the leading irrelevant interactions and corresponding coupling constants on the line of Fermi-liquid fixed points. This is done starting with the Abelian bosonization description of the QCP (Refs. 7 and 22) which uses Majorana fermions that are nonlocally related to the original Dirac fermion fields in Eq. (1). We will then see that, at temperatures lower than T^* and with the relevant operator present, single-electron scattering states become the correct particles in terms of which the FL theory is conveniently written.

A. Phase shift analysis

Before describing the derivation of the FL Hamiltonian, we present a simple derivation of the form of the phase shifts in terms of which the single-electron scattering states are defined. These are then compared to the phase shifts extracted from the fixed point NRG spectrum. Since one can derive the same form for these phase shifts from the fixed-point analysis described at the end of this section, numerical confirmation of the phases shifts provides additional support for the analytic calculation of the FL Hamiltonian.

In the simpler FL theory of the single-channel Kondo effect,[23] the Hamiltonian is written in terms of weakly interacting fermionic scattering states which are simply the original Dirac electrons in which the zero-temperature scattering phase shift is incorporated. The same holds true for the two-impurity model under consideration. Using the $L \leftrightarrow R$ symmetry, the original Dirac fermions satisfy a FL boundary condition (BC),

$$(\psi_{L\mu} + \psi_{R\mu})(0^+) = e^{2i\delta_e}(\psi_{L\mu} + \psi_{R\mu})(0^-),$$

$$(\psi_{L\mu} - \psi_{R\mu})(0^+) = e^{2i\delta_o}(\psi_{L\mu} - \psi_{R\mu})(0^-). \tag{15}$$

In our chirality convention for the one-dimensional fields, the region $x>0 (x<0)$ corresponds to the incoming (outgoing) part of the field. Furthermore, using the special particle-hole symmetry

$$\psi_{L\mu} \to \psi^\dagger_{L\mu}, \quad \psi_{R\mu} \to -\psi^\dagger_{R\mu}, \tag{16}$$

it follows[18] that $\delta_e=-\delta_o \equiv \delta$.

To calculate the phase shift δ, we use its relation to the zero-temperature conductance[3]

$$\frac{h}{2e^2}G = \sin^2(\delta_e - \delta_o) = \sin^2 2\delta. \tag{17}$$

Comparing this with[7]

$$G = \frac{2e^2}{h}\frac{T_{LR}}{T^*}, \tag{18}$$

we can immediately extract the form of δ,

$$\delta = \frac{1}{2}\arg(\sqrt{T_{\delta K}} + i\sqrt{T_{LR}}) = \frac{1}{2}\arg\left(\sqrt{\frac{a}{b}}\frac{K-K_c}{T_K} + i\nu V_{LR}\right), \tag{19}$$

where, in the last equality, we have substituted the expressions for $T_{\delta K}$ and T_{LR} from Eq. (6).

For $V_{LR}>0$, the phase shift δ changes from 0 to $\pi/2$ as function of K, and it takes the value of $\pi/4$ at $K=K_c$. This agrees with the numerical results of Jones *et al.*[9] While the original electrons suffer a phase shift, the single-particle scattering states $\Psi_{j\mu}$ incoming from lead $j=1,2=(L,R)$, defined by

$$\Psi_{j\mu}(x) = \theta(x)\psi_{j\mu}(x) + \sum_{j'} \theta(-x)s_{jj'}\psi_{j'\mu}(x),$$

$$s = \begin{pmatrix} \cos 2\delta & -i\sin 2\delta \\ -i\sin 2\delta & \cos 2\delta \end{pmatrix}, \tag{20}$$

are continuous at the origin: $\Psi_{i\mu}(0^+)=\Psi_{i\mu}(0^-)$.

The form of this predicted phase shift, Eq. (19), can be compared with the phase shift derived from the NRG fixed-

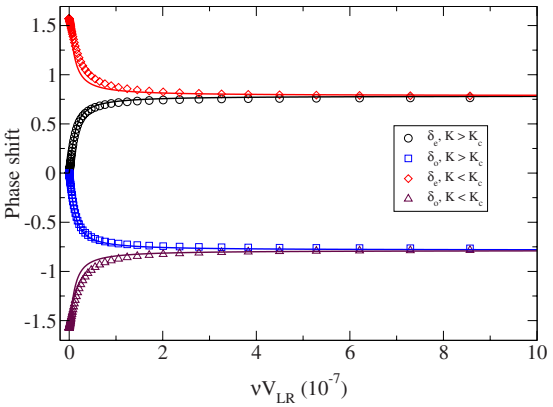

FIG. 6. (Color online) The phase shifts δ_e and δ_o in the even and odd channels (respectively) of the FL fixed point as derived from the NRG (points) with $\nu J=0.15$ as well as those phase shifts predicted analytically by Eqs. (15) and (19) (lines). The values for T_K, K_c, a, and b appearing in Eq. (19) are taken from the $\nu J=0.15$ line of Table I. We have done this for both the LSP, $K=1.30096478\times10^{-3}>K_c$, and the KSP, $K=1.30096452\times10^{-3}<K_c$.

point spectrum. To extract the phase shift, one looks at the many-body NRG energy spectrum for the Hamiltonian H_N of Eq. (8) where N is large enough such that the RG has reached one of the FL fixed points. Unlike the QCP, the LSP and KSP many-body spectra are made up of two channels of single-particle/hole excitations combined in such a way so as to respect Fermi statistics. By looking at the quantum numbers of the lowest many-body NRG energy levels, one can determine the two lowest single-particle/hole excitations η_{1p} and η_{2p} in each of the $p=e$ (even), o (odd) channels. From these we define the phase shift as

$$\delta_p = Q_{1p}\frac{\eta_{1p}}{\eta_{1p}+\eta_{2p}}\pi \tag{21}$$

for the case of even N. Here, $Q_{1p}=\pm1$ is the charge of the lowest excitation in the p channel indicating whether the spectrum is shifted up $(Q_{1p}=1,\delta_p>0)$ or down $(Q_{1p}=-1,\delta_p<0)$ relative to the spectrum with $V_{LR}=0$. The η's are marked in Fig. 1. The definition for odd N is simply shifted by $\pi/2$. This definition of the phase shift at the fixed point follows closely that used in Ref. 24 for a model of a quantum dot in an Aharonov-Bohm ring.

In Fig. 6, we have plotted the phase shifts as derived in this way from the NRG and compared them with those predicted from Eq. (19) for both $K>K_c$ and $K<K_c$. We find the agreement to be quite good and take this as support for our analysis of the FL fixed point.

Slight deviations from the continuum model used to derive Eq. (19) are known to exist due to the fact that $\Lambda>1$ in the discrete NRG Hamiltonian (see Ref. 24 for a discussion of this effect). Furthermore, we obtain better agreement with the NRG for the phase shifts in the LSP than we do for phase shifts in the KSP. The nature of this discrepancy looks very similar to that due to the presence of an additional potential scattering term that is generated by the Kondo interaction in the screening channel when particle-hole symmetry is broken.[24,25] Since the presence of a nonzero V_{LR} breaks particle-hole symmetry, one would expect such an effect but only in the KSP where Kondo screening occurs. This is precisely what is seen in Fig. 6. However, the form of this additional potential scattering was only derived for single-channel, single-impurity models[24,25] so more analysis is required to determine for certain if this is the nature of the discrepancy in the KSP phase shifts. Nevertheless, it is clear that Eq. (19) captures the leading order contribution to the phase shift for the entire manifold of fixed points.

B. Fermi-liquid hamiltonian

We now turn our attention to the derivation of the FL Hamiltonian. Using Abelian bosonization, one can write the original free fermion theory [Eq. (1) with $J\to0$ and $V_{LR}\to0$] in terms of eight chiral Majorana fermions χ_i^A associated with the real $(\chi_1^A=\frac{\psi_A^\dagger+\psi_A}{\sqrt{2}})$ and imaginary $(\chi_2^A=\frac{\psi_A^\dagger-\psi_A}{\sqrt{2}i})$ parts of the charge, spin, flavor, and spin-flavor fermions $\psi_A\sim e^{-i\phi_A}$, $(A=c,s,f,X)$. The bosonic fields ϕ_A are linear combinations of the four bosonic fields associated with the original Dirac fermions, $\psi_{i\mu}\sim e^{-i\phi_{i\mu}}$, $(i=L,R=1,2,\mu=\uparrow,\downarrow=1,2)$ given by $\{\phi_c,\phi_s,\phi_f,\phi_X\}=\frac{1}{2}\Sigma_{i\mu}\phi_{i\mu}\{1,(-1)^{\mu+1},(-1)^{i+1},(-1)^{\mu+i}\}$.

The free Hamiltonian is $H_0[\{\chi'\}]=\frac{i}{2}\Sigma_{j=1}^8\int dx\chi_j'\partial_x\chi_j'$, where $\{\chi_1',\ldots,\chi_8'\}=\{\chi_2^X,\chi_1^f,\chi_2^f,\chi_1^X,\chi_1^c,\chi_2^c,\chi_1^s,\chi_2^s\}$ is an arbitrary relabeling of the eight fields. Turning on the Kondo coupling J at $V_{LR}=0$, the QCP is obtained at $K=K_c$. It is described simply in terms of a change in the BC relative to the free case in which $\chi_i'(0^-)=\chi_i'(0^+)$, $(i=1,\ldots,8)$. The change in BC occurs only for the first Majorana fermion, $\chi_1'(0^-)=-\chi_1'(0^+)$.

For energies $\ll T_K$, we define a new basis,

$$\chi_1(x)=\chi_1'(x)\mathrm{sgn}(x),$$

$$\chi_i(x)=\chi_i'(x)\quad(i=2,\ldots,8) \tag{22}$$

and write the leading terms in the Hamiltonian describing deviations from the QCP due to finite $K-K_c$ as well as finite V_{LR} as $H_{\mathrm{QCP}}=H_0[\{\chi\}]+\delta H_{\mathrm{QCP}}$ with[7]

$$\delta H_{\mathrm{QCP}}=\sum_{i=1}^{2}\lambda_i\chi_i(0)d\text{-}d^\dagger\sqrt{2}. \tag{23}$$

Here, d is a local complex fermion, $a^2=1/2$. Both terms in δH_{QCP} have critical dimension 1/2 so that they destabilize the QCP. The coupling constants satisfy $\lambda_1\propto K-K_c$, $\lambda_2\propto V_{LR}$ and

$$T_{\delta K}=\lambda_1^2,\quad T_{LR}=\lambda_2^2,\quad T^*=\lambda_1^2+\lambda_2^2, \tag{24}$$

where T^* is also given in Eq. (3) with the coefficients a and b determined numerically in Table I. Below the crossover scale T^*, the system flows to FL fixed points whose nature depend on the ratio λ_1/λ_2.

The crucial observation is that only the linear combination $[\lambda_1\chi_1(x)+\lambda_2\chi_2(x)]/\lambda$ of the eight Majorana fermions at the quantum critical point participates in this crossover. Here $\lambda=\sqrt{\lambda_1^2+\lambda_2^2}$. It can be shown that the effect of δH_{QCP} is to modify the BC for only this linear combination by a simple sign change at the boundary, $[\lambda_1\chi_1(0^+)+\lambda_2\chi_2(0^+)]/\lambda=$

$-[\lambda_1\chi_1(0^-)+\lambda_2\chi_2(0^-)]/\lambda$. In order to write down the FL fixed-point Hamiltonian, we define a new basis with modified BC, $\{\eta\}$, where

$$\eta_1(x) = \mathrm{sgn}(x)[\lambda_1\chi_1(x) + \lambda_2\chi_2(x)]/\lambda,$$

$$\eta_2(x) = [-\lambda_2\chi_1(x) + \lambda_1\chi_2(x)]/\lambda,$$

$$\eta_i(x) = \chi_i(x) \quad (i = 3, \ldots, 8). \tag{25}$$

We can therefore write the Hamiltonian for the FL fixed points as $H_{\mathrm{FL}}=H_0[\{\eta\}]+\delta H_{\mathrm{FL}}$. For clarity, we recapitulate the notation: in the weak-coupling regime we defined the set of Majorana fermions $\{\chi'\}$; in the QCP, the Hamiltonian, Eq. (23), is written in terms of $\{\chi\}$ given by the relation, Eq. (22); in the FL regime, the Hamiltonian will be written in terms of the $\{\eta\}$ operators defined in Eq. (25).

Near a FL fixed point the leading interactions have scaling dimension 2 . In our local theory, the interaction δH_{FL} acts only at $x=0$ and involves uniquely η_1 which is the only field participating in the crossover in Eq. (23). The only possible such operator is

$$\delta H_{\mathrm{FL}} = \lambda_{\mathrm{FL}} i\eta_1\partial_x\eta_1|_{x=0}. \tag{26}$$

In the FL theory, T^* acts as a high-energy cutoff. From dimensional analysis, the coupling constant scales as $\lambda_{\mathrm{FL}}\sim\frac{1}{T^*}$. Since Eq. (23) is quadratic, we can determine the coefficient exactly by matching at low temperatures the results of calculations of a physical quantity (e.g., the conductance of a quantum dot[7]) as calculated either using Eq. (23) or Eq. (26). In this way, we obtain $\lambda_{\mathrm{FL}}=\frac{4}{T^*}$.

We have derived the FL scattering states $\Psi_{j\mu}$, $j=1,2=L,R$, in Eq. (20) and now rewrite the FL interaction of Eq. (26) in terms of them. First we write δH_{FL} using Eqs. (22) and (25) as

$$\delta H_{\mathrm{FL}} = \frac{4i}{T^*}\Big[\cos^2(2\delta)(\chi_1' i\partial_x\chi_1') + \sin^2(2\delta)(\chi_2' i\partial_x\chi_2') + \mathrm{sgn}(x)\frac{1}{2}\sin(4\delta)(\chi_1' i\partial_x\chi_2' + \chi_2' i\partial_x\chi_1')\Big]. \tag{27}$$

These quadratic operators of dimension 4 can be written as a product of two normal ordered quadratic forms using

$$\chi_1' i\partial_x\chi_1' + \chi_2' i\partial_x\chi_2' = (i{:}\chi_1'\chi_2'{:})^2,$$

$$\chi_1' i\partial_x\chi_1' - \chi_2' i\partial_x\chi_2' = (i{:}\chi_1'\chi_3'{:})^2 - (i{:}\chi_2'\chi_3'{:})^2,$$

$$\chi_1' i\partial_x\chi_2' + \chi_2' i\partial_x\chi_1' = \{{:}\chi_1'\chi_3'{:},{:}\chi_3'\chi_2'{:}\}_+, \tag{28}$$

where $\{,\}_+$ stands for the anticommutator.

These normal ordered quadratic forms are related to the flavor currents,

$$\vec{J}_f = \sum_{\mu,i,j} {:}\Psi_{i\mu}^\dagger \frac{\vec{\tau}_{ij}}{2}\Psi_{j\mu}{:}, \tag{29}$$

where $\vec{\tau}_{ij}$ are Pauli matrices. Indeed in the range $x>0$ at which the scattering states coincide with the original fermions $\Psi(x>0)=\psi(x>0)$, these can be expressed as

$$J_f^x = i{:}\chi_1'\chi_2'{:}, \quad J_f^y = i{:}\chi_1'\chi_3'{:}, \quad J_f^z = i{:}\chi_3'\chi_2'{:}. \tag{30}$$

Using Eqs. (27), (28), and (30), we finally obtain

$$\delta H_{\mathrm{FL}} = \frac{2}{T^*}\vec{J}_f^T\hat{M}\vec{J}_f, \tag{31}$$

where

$$\hat{M} = \begin{pmatrix} 1 & 0 & 0 \\ 0 & \cos 4\delta & -\sin 4\delta \\ 0 & -\sin 4\delta & -\cos 4\delta \end{pmatrix}.$$

One can see that, due to the potential scattering term $\propto V_{LR}J_f^x$, the flavor SU(2) symmetry is reduced down to U(1). One can rewrite δH_{FL} in different ways, for example, in Ref. 7, the same equation is written in an explicitly spin SU(2) symmetric way.

We emphasize the universality of the derived FL Hamiltonian: for any value of the ratio of original parameters $V_{LR}/(K-K_c)$, all coupling constants of H_{FL} are determined up to the overall energy scale T^* which was calculated numerically here. The universality follows from strong restrictions due to a large symmetry that emerges close to the quantum critical point[21] and leads to the simple form of H_{QCP} in Eq. (23). One can see that H_0^{QCP} has an SO(8) symmetry. Due to δH_{QCP}, the crossover from the QCP to FL fixed points has an SO(7) symmetry represented by rotations of the vector $(\eta_2,\ldots,\eta_8)$. This symmetry considerably restricts the possible interactions and sets relations between the different coefficients in Eq. (31). The conditions of validity of δH_{FL} is small deviations from the QCP $|K-K_c|\ll T_K$, $\nu V_{LR}\ll 1$. In addition, a scale separation $T^*\ll T_K$ is required. This scale separation was shown to hold using our NRG calculations as discussed in detail in Sec. II.

In practice, the SO(8) symmetry at the quantum critical point is broken by marginal and irrelevant operators at the QCP such as the leading irrelevant operator $(\partial_x\chi_1)$ at the quantum critical point. However, these will be associated with a small parameter $1/T_K$ and, hence, are neglected at $T^*\ll T_K$. For finite V_{LR} or $K-K_c$, additional marginal and irrelevant terms are produced at the quantum critical point, part of which were present before. However, close enough to the quantum critical point, namely, for $\nu V_{LR}\ll 1$ and $|K-K_c|\ll T_K$, those perturbations can be safely ignored.

IV. COMPARISON WITH PREVIOUS NRG RESULTS

We now compare our description of the crossover scale to that obtained from previous NRG research.[10,11] Since the $K-K_c$ dependence of T^* is well established, we focus on $T_{LR}=bT_K(\nu V_{LR})^2$. Given that the earlier papers[10,11] present NRG calculations on the Anderson model, we will re-express our Kondo model results in terms of Anderson model parameters.[7] We define the Anderson model with hopping t_d between the conduction electrons and the impurities and hopping t_{LR} between the two impurity sites on which there is a Coulomb repulsion U and resonant energy level $\varepsilon_d=-U/2$. The Kondo parameters are given by

$$J \approx 8t_d^2/U,$$

$$K \approx 4t_{LR}^2/U,$$

$$V_{LR} \approx 4t_d^2 t_{LR}/U^2 \approx t_{LR}J/(2U),$$

$$T_K \approx U\sqrt{\frac{\pi\nu J}{16}}\exp\left(-\frac{1}{\nu J}\right). \tag{32}$$

(See Ref. 26 for the final formula which is the same as that used in Ref. 11.) Using this correspondence, the crossover temperature is

$$T_{LR} = \frac{bT_K(\nu J)^2}{4U^2}t_{LR}^2. \tag{33}$$

Evaluated at $t_{LR}=t_{LR}^c \equiv \sqrt{UK_c/4}$ and estimating $K_c = 4(t_{LR}^c)^2/U \approx 3T_K$ and $b \approx 115$, we obtain

$$\frac{T_{LR}}{T_K} \approx 20\frac{T_K(\nu J)^2}{U}. \tag{34}$$

Izumida and Sakai[11] calculate, using the NRG, the linear conductance both at $T=0$ as a function of t_{LR} as well as at $t_{LR}=t_{LR}^c$ as a function of T. In both cases, we compare their NRG conductance results with the expression derived in Ref. 7, where the nonlinear conductance is written explicitly in terms of the crossover scales T^* and T_{LR}. In the limit of linear conductance and $T \ll T^*$, this is given by[7]

$$G = \frac{2e^2}{h}\frac{T_{LR}}{T^*}\left[1-\left(\frac{2\pi T}{\sqrt{3}T^*}\right)^2\right]. \tag{35}$$

As discussed in the previous section, the $T=0$ limit of this expression for the conductance agrees well with our NRG results on the Kondo model.

We first look at the t_{LR} dependence of the $T=0$ linear conductance which will have a peak in the conductance centered around $t_{LR}=t_{LR}^c$. From Eqs. (18), (32), and (33), we see that the width of this peak is given by

$$\delta t_{LR}/t_{LR}^c \approx (1/2K_c)\sqrt{T_K T_{LR}/a} \propto \sqrt{T_{LR}/T_K}. \tag{36}$$

In Ref. 11, the $T=0$ linear conductance is calculated by extracting the effective parameters of the Fermi-liquid theory from the finite-size NRG spectrum of the Anderson model. From their Fig. 1 which uses $U=0.1$ and parameters that give $\nu J=0.12$, one observes that

$$\delta t_{LR}/t_{LR}^c \approx 1 \tag{37}$$

resulting in

$$T_{LR} \approx T_K. \tag{38}$$

For comparison, in Fig. 7, we have plotted Eq. (18) as a function of $t_{LR}-t_{LR}^c$ using $U=0.1$ and Eq. (32) for T_K as in Ref. 11 and parameters (a,b,K_c) interpolated from Table I. From the $\nu J=0.12$ curve, we obtain

$$\delta t_{LR}/t_{LR}^c \approx 10^{-4}, \tag{39}$$

which implies

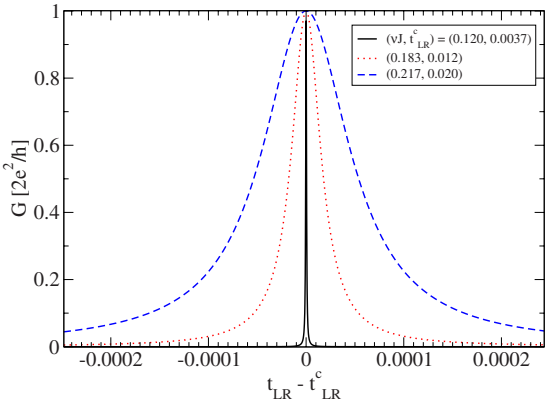

FIG. 7. (Color online) The zero-temperature conductance of Eq. (35) plotted as a function of $t_{LR}-t_{LR}^c$ using the correspondence between Kondo and Anderson model parameters described in the text. This is to be compared to a similar plot in Fig. 1 of Ref. 11. We have used Eqs. (3), (6), and (35), the values of a and b listed in the first three lines of Table I and $U=0.1$ as in Ref. 11.

$$T_{LR} \approx 10^{-8}T_K. \tag{40}$$

That is, our result for the crossover scale differs by 8 orders of magnitude from that inferred from Ref. 11. It is possible that this large discrepancy reflects the difference between Kondo and Anderson models though this seems unlikely.

Izumida and Sakai also calculate the finite-temperature conductance at $t_{LR}=t_{LR}^c$ using a Kubo formula in terms of the energy eigenvalues and eigenvectors as computed in the NRG using the same values of U and νJ discussed above. We can extract an estimate of T_{LR} using Eq. (35) with $T^* = T_{LR}$. From the lowest temperature data in Fig. 5 of Ref. 11, we estimate

$$T_{LR} \approx 8 \times 10^{-8} \approx 0.02T_K. \tag{41}$$

This is significantly different than the estimate obtained from the $T=0$ linear conductance above. The fact that the two estimates of T_{LR} obtained from Ref. 11 do not agree violates the scaling behavior that we expect. Recall that in the previous section, we have checked the scaling hypothesis through our calculation of the dependence of the phase shifts obtained via the NRG on K and V_{LR}.

Sakai and Shimizu[10] report that the energy scale of T_{LR} is in fact

$$T_{LR} = 2 \times 10^{-3}\frac{t_{LR}^2}{T_K}. \tag{42}$$

This estimate is derived from their numerical calculation of the susceptibility $\chi_a(\omega)$ of the antiferromagnetic moment $(S_1^z - S_2^z)/\sqrt{2}$ and comparing it to the ferromagnetic impurity susceptibility $\chi(\omega)$. It follows from Ref. 18 that, when $\omega, T \ll T^* \ll T_K$, $\mathrm{Im}\,\chi \sim \omega/T_K^2$ and $\mathrm{Im}\,\chi_a \sim \omega/(T^*T_K)$. Hence, the crossover scale T_{LR} can be estimated by

$$\lim_{\omega\to 0}\frac{\mathrm{Im}\,\chi}{\omega}\Big/\lim_{\omega\to 0}\frac{\mathrm{Im}\,\chi_a}{\omega} = \frac{T_{LR}}{T_K}, \tag{43}$$

which is how the authors obtained Eq. (42).

Setting $t_{LR}=t_{LR}^c$ and estimating $K_c \approx 3T_K$, this estimate of T_{LR} is

$$\frac{T_{LR}}{T_K} \approx 10^{-3}\frac{U}{T_K}. \tag{44}$$

This disagrees drastically with our estimate in Eq. (34). Not only is the magnitude of T_{LR} different than that obtained by us but their estimate decreases with increasing T_K whereas ours does the opposite. Furthermore, substituting the values of $U=0.1$, $T_K=4\times10^{-6}$ as in Ref. 11, one obtains $T_{LR} \approx 25T_K$, different from the estimates obtained in Eqs. (38) and (41). Once again, this violates the scaling hypothesis and does not even correspond to a crossover scale at all since $T_{LR} > T_K$.

Thus, the three different estimates of the crossover scale related to potential scattering by Sakai and collaborators[10,11] are all much larger than our estimate and appear inconsistent with each other. We have thoroughly established the behavior of the crossover scale for the Kondo model but similar work on the Anderson model may be required to resolve these apparent discrepancies. It is important to resolve this issue to understand the experimental feasibility of observing the QCP.

V. DISCUSSION

We have presented a detailed analytic and numerical calculation of the scale for the crossover away from the QCP in the two-impurity Kondo model. It is at this scale that the system flows to a Fermi-liquid fixed point on a one-dimensional manifold of fixed points parametrized by $V_{LR}/(K-K_c)$. The Fermi-liquid behavior along this manifold has been derived in detail and confirmed numerically. Furthermore, the more precise calculation of T^* presented in this paper provides a more accurate estimate of the linear conductance, Eq. (35), and, indeed, can be used in the more general formula for the conductance extended to higher temperatures and finite voltage bias.[7] It is known that such a Kondo model can accurately describe the behavior of quantum dots in certain parameter regimes and it is to this application that we focus our analysis.

It is interesting to discuss how our results for T^* affect the feasibility of observing the QCP in such a quantum dot experiment. The criterion for the observability of the QCP is the separation of the two crossovers, namely, the crossover from weak-coupling to QCP occurring at scale T_K and the crossover from QCP to FL occurring at scale T^*. This requirement reads $T_K/T^* \gg 1$. An expression for this ratio is given in Eq. (34).

In order to estimate the magnitude T_K/T^*, we use a typical value of $U=1.5$ meV and a value of $\nu J=0.217$. Rather than estimating T_K using the Kondo model formula (2), we use the Kondo temperature of Eq. (32) as derived from an Anderson model[26] which is more applicable to quantum dots. In this case, we obtain $T_K \approx 3.1$ μeV ≈ 0.04 K so that the ratio of scales is $T_K/T^* \approx 500 \gg 1$. Although it would be very difficult to attain temperatures $T < T_K$ for such a small value of the Kondo temperature, holding $U=1.5$ meV fixed in Eq. (34) suggests that one can obtain a ratio of $T_K/T^* \approx 10$ at a Kondo temperature of $T_K \approx 40$ μeV ≈ 0.5 K ($\nu J \approx 0.4$), a temperature that can be obtained in modern quantum dot experiments. Hence, we conclude that it is possible to realize the QCP in a double quantum dot system.

ACKNOWLEDGMENTS

The authors would like to thank Barbara Jones for helpful discussions during the course of this research. This work was supported by the Government of British Columbia (J.M.), the A.V. Humboldt Foundation (E.S.), the Natural Sciences and Engineering Research Council of Canada (I.A.), and the Canadian Institute for Advanced Research (J.M., E.S., and I.A.).

[1] P. Nozières and A. Blandin, J. Phys. (France) **41**, 193 (1980).
[2] R. M. Potok, I. G. Rau, H. Shtrikman, Y. Oreg, and D. Goldhaber-Gordon, Nature (London) **446**, 167 (2007).
[3] A. Georges and Y. Meir, Phys. Rev. Lett. **82**, 3508 (1999).
[4] G. Zaránd C.-H. Chung, P. Simon, and M. Vojta, Phys. Rev. Lett. **97**, 166802 (2006).
[5] H. Jeong, A. M. Chang, and M. R. Melloch, Science **293**, 2221 (2001).
[6] J. Bork, Y. Zhang, L. Diekhöner, P. Simon, L. Borda, J. Kroha, P. Wahl, and K. Kern (private communication).
[7] E. Sela and I. Affleck, Phys. Rev. Lett. **102**, 047201 (2009); Phys. Rev. B **79**, 125110 (2009).
[8] E. Sela and I. Affleck, Phys. Rev. Lett. **103**, 087204 (2009).
[9] B. A. Jones, C. M. Varma, and J. W. Wilkins, Phys. Rev. Lett. **61**, 125 (1988); B. A. Jones and C. M. Varma, Phys. Rev. B **40**, 324 (1989); B. A. Jones, Physica B **171**, 53 (1991).
[10] O. Sakai and Y. Shimizu, J. Phys. Soc. Jpn. **61**, 2333 (1992).
[11] W. Izumida and O. Sakai, Phys. Rev. B **62**, 10260 (2000).
[12] K. G. Wilson, Rev. Mod. Phys. **47**, 773 (1975).
[13] H. R. Krishna-murthy, J. W. Wilkins, and K. G. Wilson, Phys. Rev. B **21**, 1003 (1980).
[14] H. R. Krishna-murthy, J. W. Wilkins, and K. G. Wilson, Phys. Rev. B **21**, 1044 (1980).
[15] R. Bulla, T. A. Costi, and T. Pruschke, Rev. Mod. Phys. **80**, 395 (2008).
[16] Only the lowest M eigenvalues are kept at each iteration to prevent the Hilbert space from growing exponentially with increasing N. We take $M=3500$ (only counting those states that are not related to others by symmetry so that we are really considering more than 3500 states as described in Ref. 9) and find that our results do not change if more states are kept.
[17] Or, more precisely, when the energy spectrum of $\{H_N, H_{N+2}, H_{N+4}, \ldots\}$ remains the same.
[18] I. Affleck, A. W. W. Ludwig, and B. A. Jones, Phys. Rev. B **52**, 9528 (1995).
[19] We obtain K_c numerically to 8–9 significant digits.

[20] We use the extrapolated points rather than all of the data to avoid discrepancies due to deviations of T^* away from $(\nu V_{LR})^2$ behavior for large νV_{LR}.
[21] I. Affleck and A. W. W. Ludwig, Phys. Rev. Lett. **68**, 1046 (1992).
[22] J. Gan, Phys. Rev. Lett. **74**, 2583 (1995); Phys. Rev. B **51**, 8287 (1995).
[23] P. Nozières, J. Low Temp. Phys. **17**, 31 (1974).
[24] J. Malecki and I. Affleck, Phys. Rev. B **82**, 165426 (2010).
[25] D. M. Cragg and P. Lloyd, J. Phys. C **11**, L597 (1978); **12**, 3301 (1979).
[26] F. D. M. Haldane, J. Phys. C **11**, 5015 (1978).